Electrochimica Acta 319 (2019) 690–704

Contents lists available at ScienceDirect

Electrochimica Acta

journal homepage: www.elsevier.com/locate/electacta

Influence of water content and applied potential on the electrodeposition of Ni coatings from deep eutectic solvents

Monika Lukaczynska [a], El Amine Mernissi Cherigui [a], Andrea Ceglia [b], Krista Van Den Bergh [c], Joost De Strycker [c], Herman Terryn [a], Jon Ustarroz [a, d, *]

[a] Research Group Electrochemical and Surface Engineering (SURF), Vrije Universiteit Brussel, Pleinlaan 2, 1050, Brussels, Belgium
[b] Department of Applied Physics and Photonics, B-PHOT Research Group, Vrije Universiteit Brussel, Pleinlaan 2, 1050, Brussels, Belgium
[c] OCAS n.v., President John F. Kennedylaan 3, 9060, Zelzate, Belgium
[d] Chemistry of Surfaces, Interfaces and Nanomaterials (ChemSIN), Université Libre de Bruxelles, Boulevard du Triomphe 2, 1050, Brussels, Belgium

ARTICLE INFO

Article history:
Received 9 January 2019
Received in revised form
26 June 2019
Accepted 27 June 2019
Available online 2 July 2019

Keywords:
Nickel
Steel
Electrodeposition
Deep eutectic solvents
Choline chloride-urea

ABSTRACT

Ni coatings were electrodeposited from 1:2 choline chloride (ChCl) - urea (U) deep eutectic solvents (DESs) on low carbon steel. We report on the inter-related influence of water content in the electrolyte and applied potential on the formation of Ni films and their chemical composition and morphology. This was investigated by cyclic voltammetry (CV) and chronoamperometry (CA) in combination with ex-situ characterization techniques (FE-SEM, EDS, XPS and Raman spectroscopy). Ni electrodeposition from DES is shown to be highly complex: Ni^{+2} reduction is followed by water reduction, which triggers electrolyte decomposition. A water content higher than 4.5%*wt* and/or performing electrodeposition at potentials more negative than $E = -0.90V$ vs Ag quasi-reference electrode enhances the decomposition of the solvent. This breakdown appears via either an electrochemical reaction or triggered by water splitting. In both cases, it leads to the incorporation of DESs decomposition products, such as trimethylamine and acetaldehyde within the Ni film. Under these conditions, the films are composed of metallic Ni and $NiO_x(OH)_{2(1-x)}$.

1. Introduction

Nickel-coated steel is used in a wide range of applications, such as batteries, electronic elements, telecommunications devices, and automotive and aviation components [1]. This is due to its high corrosion resistance, which is similar to this of stainless steel, but features better machinability, weldability and wear resistance [2,3]. Nickel and its alloys are generally deposited on steel via an electroless or an electrochemical route. Although the electroless process provides coatings with good protective and functional properties [2,4], electrodeposition offers many possibilities to tune the chemical composition, morphology and structure of the deposited films [5,6].

Nickel electroplating is generally performed in the Watts bath, an aqueous solution consisting of $NiCl_2 \cdot 6H_2O$, $NiSO_4 \cdot 6H_2O$ and H_3BO_3 [1,7]. For the coatings to feature the required chemical composition, structure and mechanical properties, these baths usually contain several additives, such as benzene sulphonic acid, p-toluene sulphonamide, saccharin, coumarine, thiourea, etc. [1,7–9]. Some of these additives (*i.e.* thiourea) can be harmful. Additionally, slight changes in the additive purity or concentration can lead to morphological issues in the deposited films, such as lack of adhesion, pitting, blistering or brittleness [1,8]. Furthermore, since nickel has a considerably negative standard reduction potential, $E_{Ni^{2+}/Ni^0} = -0.25V$ vs SHE, and is catalytic towards the production of hydrogen through water electrolysis, electrodeposition from aqueous solutions is usually complicated and involves a low cathodic current efficiency and results in cracked, porous and brittle films [1].

To decrease hydrogen evolution and its negative effect on the properties of the deposited coatings, and to reduce the number of additives used in aqueous electrolytes, room temperature ionic liquids (RTILs) are interesting alternatives for the electrodeposition of highly electronegative metals, such as Al, Mg, Ni, due to their

* Corresponding author. Research Group Electrochemical and Surface Engineering (SURF), Vrije Universiteit Brussel, Pleinlaan 2, 1050, Brussels, Belgium.
E-mail address: jon.ustarroz@vub.be (J. Ustarroz).

https://doi.org/10.1016/j.electacta.2019.06.161
0013-4686/

wide potential window (5–7*V*) [10,11]. As such, nickel coatings have been successfully obtained from 2-hydroxyethyl ammonium formate (2-HEAF) [12], 1-ethyl-3-methylimidazolium-dicyanamide [13] or 1-butyl-1-methylpyrrolidinium bis-(trifluoromethylsulfonyl)amide (BMPTFSA) [14] ionic liquids. However, their cost is substantially high and they require a constantly controlled atmosphere, which complicates their use in an industrial scale for the steel electroplating processes.

Over the past decade, deep eutectic solvents (DESs) have gained popularity and have become a promising alternative to traditional aqueous electrolytes and RTILs [15–19]. The electrochemical potential window of these solvents, although not as large as this of RTILs, allows, in principle, reducing Ni^{2+} without water splitting and hydrogen gas formation [20,21]. Similarly to RTILs, DESs have negligible vapour pressure and high thermal stability. Interestingly, DESs are attractive for large-scale industrial applications because they are easier to prepare and cheaper than ILs. Additionally, they are known to be non-hazardous solvents [17–19,22].

In the past few years, the electrodeposition of Ni from DESs has been shown to be feasible on a wide variety of substrates such as Pt [21,23], Cu [24], glassy carbon (GC) [25–27], Al [28], brass [29], etc. A wide range of morphologies (supported nanoparticles [25–27] or thin films [23,24]), structures (pellets, nodules, dendrites, etc. [20,30]) as well as chemistries (metallic nickel [24,30], nickel oxide [29,31], nickel hydroxide [25,26]) can be obtained.

In this context, it is highly relevant to understand the hygroscopic nature of DESs and its effect on the electrodeposition mechanism. On the one hand, the presence of small amounts of water (up to 6 *wt%*) has recently been proposed to be beneficial due to the decrease of viscosity and increase of conductivity that originate from increasing the ion mobility in the electrolyte [32–35]. Furthermore, by changing and controlling the water content, it is possible to tailor the morphologies and structures of the deposited coatings: pellet-like, nodular, or cauliflower-like [34,36]. On the contrary, the hygroscopicity of DESs might be disadvantageous as the increase of water content may cause a decrease of the electrochemical potential window [33,34]. Essentially, since water electrolysis may easily be triggered at the potentials where nickel is being reduced [5] and DESs are never water-free, understanding the effect of water splitting on these type of electrolytes and the electrodeposition process is of high importance [27,33–37].

Therefore, despite a large number of studies on Ni electroplating from DESs [15,21,23–37], the fundamental processes that determine the film formation and its properties are not fully understood yet. More importantly, although the number of fundamental studies on Ni electrodeposition from DESs has recently increased substantially, only a small number of studies have been reported on steel electroplating from any type of RTILs or DESs [21,24,38].

In this paper, we study the electroplating of Ni films on low carbon steel from 1:2 choline chloride (ChCl) - urea (U) DESs. We emphasize on understanding the influence of the water content, the applied potential, and their inter-related effect on the electrodeposition process. This has been accomplished by combining standard electrochemical techniques (cyclic voltammetry (CV) and chronoamperometry (CA)) with a wide range of ex-situ characterization methods such as field emission scanning electron microscopy (FE-SEM), energy dispersive X-ray (EDS), X-ray photoelectron (XPS) and Raman spectroscopy. Special attention was given to the interaction between the solvent, water, and the growing Ni phase. This article not only provides novel information on the electrochemical deposition of nickel on a technologically relevant substrate such as low carbon steel, but also provides important knowledge on the role of water and applied potential during metal electroplating process from DESs.

2. Experimental

2.1. DESs preparation

Choline chloride (Sigma – Aldrich, 98%) and urea (Merck KGaA, >99.5%) were used as received. The electrolytes were prepared by stirring these two components together at 80 °C in a 1:2 molar ratio, respectively, until obtaining a transparent homogeneous liquid phase. The addition of 0.2 M nickel chloride hexahydrate (Merck KGaA, 98%) changed the solvent color to intensive green. Additional water in certain amounts was introduced to these mixtures in the form of 0.2 M aqueous solution of nickel chloride (to preserve the nickel chloride concentration) and stirred for 24 h at room temperature to obtain a homogeneous liquid. The water content was always monitored by performing coulometric Karl Fischer titration (Metrohm KF Titrino plus: 899 Coulometer). Viscosity and conductivity of the electrolytes were measured with a rheometer (ARES rheometer) and a conductivity meter (YOKOGAWA Model SC82), respectively. In order to detect the influence of water content on the complexation of Ni in DESs, UV-Vis spectrometry measurements were performed at 60°C by using UV-Vis Avantes NIR spectrometer and a quartz cuvette with a 5 mm light path.

2.2. Electrochemistry

The electrochemical behaviour of Ni was investigated by performing cyclic voltammetry (CV) and chronoamperometry (CA). All measurements were carried out using an Autolab PGSTAT 100 potentiostat in a standard three-electrode cell configuration. In order to avoid a junction potential and due to the electrochemical stability proven earlier [15,26], an Ag wire immersed in the electrolyte was used as a quasi-reference electrode (QRE). A dimensionally stable anode (DSA) (Ti/RuO_2) was used as a counter electrode (CE) owing to its chemical and electrochemical stability in highly chlorinated electrolytes. The use of a DSA prevents the uncontrollable chemical dissolution of the anode into the bath [39]. The working electrode (WE) was a 6 mm diameter low carbon steel rod embedded in a PEEK resin. Before the measurements, the WEs were polished with 9 μm and 3 μm silica paper, followed by 0.25 μm diamond paste. Then, they were rinsed with distilled water and dried with air.

Thick coatings were obtained by a potentiostatic electrodeposition for 45 min at different potentials. Prior the use, steel sheets with dimensions of 3.5 cm × 3.5 cm were sonicated in isopropanol for 15 min. The next step consisted of degreasing in hot (60 °C) 1 M NaOH solution for 5 min, which was followed by chemical etching in 15 % HCl solution for 3 min. After each step the samples were rinsed in hot (60 °C) and room temperature water.

All electrochemical experiments were conducted at 60 °C in 1ChCl:2U containing 0.2 M $NiCl_2 \cdot 6H_2O$ and 2.1 *wt%*, 4.5 *wt%* and 7.5 *wt%* of water. Its content was quantified by Karl Fischer titration while performing the electrochemical measurements. In order to limit the concentration of water, a set of electrochemical measurements were also performed in an argon controlled atmosphere glovebox (JACOMEX GP[CONCEPT]) [27].

2.3. Surface analysis

The chemical composition of the thick Ni coatings was analysed by X-ray photoelectron spectroscopy (XPS) using a PHI Quantera SXM with an Al filament of 1486.6 eV energy, by Raman spectroscopy using an Horiba Raman microscope LabRAM HR Evolution and by energy-dispersive X-ray spectroscopy (EDS). The surface morphology of the coatings and cross-section was investigated by

field emission - scanning electron microscopy (FE-SEM) with a Jeol JSM-7100F microscope.

3. Results and discussion

3.1. Ni electrodeposition on low carbon steel: influence of water content and applied potential

Fig. 1(a) shows the cyclic voltammograms (CVs) obtained from 1ChCl:2U DESs with and without the addition of 0.2 M of $NiCl_2 \cdot 6H_2O$, as well as with different amounts of water. The inset in this figure shows the CVs of the blank electrolyte containing different H_2O contents, whose concentration was determined by the Karl Fischer measurements before and after the experiments. The upper potential limit was set at $E = 0.1V$ to avoid the anodic oxidation of steel, whereas the lower potential limit was set at $E = -1.5V$ in order to obtain information about the different cathodic reactions. In the inset of Fig. 1(a), no significant reduction peaks are observed in the CVs of the blank electrolyte containing only residual water (0.25 *wt%*), except from a small but broad shoulder with onset potential $E \approx -0.8V$. The addition of extra water (total values of 4.2 *wt%* and 7.2 *wt%*) results in a sharp increase of the cathodic current at $E \approx -1.15V$ and pronouncing the shoulder at $E \approx -0.80V$. Interestingly, the CV recorded in the glovebox (green curve in Fig. 1(a)) shows that the currents are slightly higher than these obtained for the blank solution with just residual water. This will be further discussed later in the manuscript.

The addition of 0.2 M $NiCl_2 \cdot 6H_2O$ (black curve in Fig. 1(a)) results in the electrochemical reduction of nickel (Eq. (1)):

$$Ni^{2+} + 2e^- \rightarrow Ni^0 \quad (1)$$

with an onset potential $E \approx -0.70V$ and a current maximum at $E \approx -0.95V$. A slight and broad shoulder is evidenced at a potential range from $E \approx -0.99V$ to $-1.05V$, which is followed by a sharp increase of the cathodic current, starting at $E \approx -1.07V$. The absence of anodic Ni oxidation is logical since it occurs at $E \geq 0.15V$ [26].

The increase of water content in the nickel-containing electrolyte (blue and red curves of Fig. 1(a)) causes a shift of the onset and peak maximum potentials related to Ni^{2+} reduction to less negative potentials by 0.05*V* and 0.15*V* (blue and red curves of Fig. 1(a), respectively). Furthermore, the shoulder which appears after Ni^{2+} reduction becomes broader and its onset shifts towards more

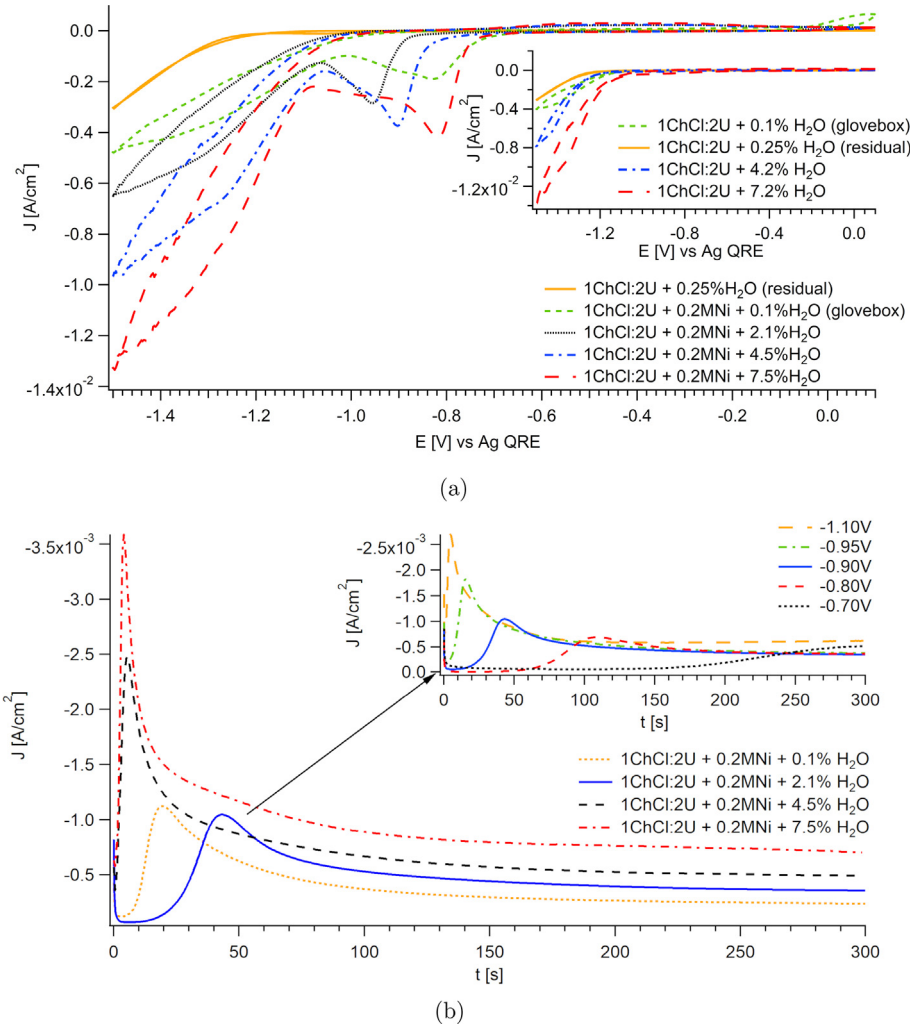

Fig. 1. (a) CVs obtained for 1ChCl:2U containing 0.2 M $NiCl_2 \cdot 6H_2O$ with different water contents. Inset: CVs obtained for blank 1ChCl:2U with different water contents. (b) CAs obtained for Ni deposition at −0.90*V* from 1ChCl:2U containing 0.2 M $NiCl_2 \cdot 6H_2O$ and different water contents. Inset: CAs obtained for deposition from 1ChCl:2U containing 0.2 M $NiCl_2 \cdot 6H_2O$ and 2.1 *wt%* water and different applied potentials.

positive potentials. Surprisingly, this tendency is not followed by the measurement in the glovebox where the DES contains only 0.1 *wt%* of water (green curve). The onset and peak potentials for nickel reduction under these conditions are similar to these obtained for 7.5 *wt%* of water (red curve). Interestingly, the onset potential of the more negative cathodic wave remains almost unaltered by the addition of water.

The fact that the nickel electrochemical reduction shifts towards less negative potentials due to addition of water (≥4.5 *wt%*) to the electrolyte is normally related to a decrease of viscosity and increase of conductivity (see Supporting Information, Table 1). In principle, such amount of H_2O is enough to solvate DES constituents and weaken the interactions between choline and urea. In this scenario, an increased water concentration will strengthen urea-urea interactions, as well as enhance the formation of hydrogen bonds between H_2O-Cl^- and H_2O-urea [40–42]. Further addition of water implies an effective aqueous solution of choline chloride and urea. These changes will significantly affect the electrochemical potential window, the onset of Ni^{2+} reduction, and ion mobility [43]. Nevertheless, the shift of the onset potential to more negative values when going from 0.1 *wt%* (glovebox) to 2.1 *wt%* is the opposite to what would be expected if conductivity was the only reason, since the conductivity for 2.1 *wt%* is 2.2 times higher than for 0.1 *wt%* (see Supporting Information, Section 1).

However, one must bear in mind that the addition of small amounts of water may also lead to changes in Ni^{2+} complexation, as well as in the structure of the electrolyte, in the bulk, and at the interface. Recently it has been shown that H_2O content significantly influences the interactions of DES constituents (water, choline, urea, chloride and nickel) [41,44,45]. Therefore, it is known that the increase of water content from 0.1 *wt%* to 2.1 *wt%* (or to 0.25 *wt%* in blank electrolyte) changes the interactions between water and DES components by possibly increasing the electrolyte integrity, which occurs by strengthening the Ch^+-Cl^- interactions [42]. This could cause the shift of Ni^{2+} reduction to more negative potentials upon presence of small amounts of water (up to ~2-3 *wt%*).

On the other hand, nickel may form different complexes in both aqueous solutions and deep eutectic solvents. In the latter case, it has been shown that the hydrogen bond donor (urea or ethylene glycol) affects the coordination of nickel in the solvent [21,46]. Therefore, it may be expected that water added to the deep eutectic solvents will behave as an additional hydrogen bond donor and significantly influences Ni complexation. To obtain insights in the nickel complexation in water containing choline chloride-urea DES, a set of UV-Vis spectroscopy measurements in 1ChCl:2U containing 0.2M $NiCl_2 \cdot 6H_2O$ and different water contents (0.1 *wt%* (glovebox), 1.4 *wt%*, 4.7 *wt%*, 7.5 *wt%* and 100 *wt%*) at 60 °C were performed (see Supporting Information, Section 2). UV-Vis indicates that, in a 1ChCl:2U DES, Ni coordination changes from a mixture of tetrahedral and octahedral at 0.1 *wt%* of water content (glovebox) to a purely octahedral for DES containing ≥ 1.4 *wt%* (outside the glovebox). The addition of extra water to the mixture up to an aqueous solution changes the nature of the ligands in the first coordination shell without affecting the octahedral geometry. This could imply that the reason why nickel reduction is easier under glovebox conditions (0.1 *wt%* H_2O) may be due to the appearance of tetrahedral coordinated nickel in these conditions.

Additionally, nickel is also known to catalyse water electrolysis, which explains the appearance of the shoulder following Ni^{2+} reduction. Once nickel nuclei are formed and water can be reduced at the nickel surface, the following reactions can be triggered: hydrogen adsorption (Eq. (2)), precipitation of nickel hydroxide in the presence of OH^- (Eq. (3)) and water electrolysis (Eq. (4)) [25,26,47].

$$Ni + H_2O + e^- \rightarrow Ni - H_{ads} + OH^- \quad (2)$$

$$Ni^{2+} + 2OH^- \rightarrow Ni(OH)_{2(ads)} \quad (3)$$

$$2H_2O + 2e^- \rightarrow H_2 + 2OH^- \quad (4)$$

For higher water contents (4.5 *wt%* and 7.5 *wt%* - blue and red curve, respectively), this shoulder is triggered at less negative potentials and becomes more significant than for 2.1 *wt%* water content (black curve). However, the magnitude of the currents, even for large amounts of water (7.5 *wt%*), indicates that this process is not bulk water electrolysis (Eq. (4)), but rather surface limited hydrogen adsorption (Eq. (2)), followed by nickel hydroxide precipitation (Eq. (3)). The process occurring at more negative potential, with onset at $E \approx -1.15V$, is normally ascribed as solvent breakdown due to the electrochemical reduction of the choline cation. However, it can be seen that after reaching $E \approx -1.30V$, $E \approx -1.26V$ and $E \approx -1.22V$ for 2.1 *wt%*, 4.5 *wt%* and 7.5 *wt%* H_2O, respectively, the current increases less sharply. Such behaviour indicates that this cathodic wave has two contributions and one of them is limited by mass transport. The most plausible explanation is that, at these potentials, choline reduction occurs together with bulk water electrolysis. The latter can be confirmed by the formation of visible hydrogen gas bubbles. The molar concentration of water is 0.12 M, 0.29 M, 2.46 M, 5.27 M and 8.79 M for 0.1 *wt%* (in blank electrolyte in glovebox), 0.25 *wt%* (in blank electrolyte), 2.1 *wt%*, 4.5 *wt%* and 7.5 *wt%*, respectively (see Supporting Information, Table 2). Therefore, bulk water electrolysis would result into cathodic currents of similar (0.1 *wt%*) or higher (2.1 *wt%*, 4.5 *wt%* and 7.5 *wt%*) magnitudes to these of nickel reduction, as it is the case. At potentials more negative than $E = -1.5V$ (not shown), the current does not become mass-transport limited and as such, implies that the electrochemical decomposition of the solvent occurs in this potential range. The cathodic breakdown of the electrolyte can follow the routes presented in Eqs. (5) and (6) [48], where Eq. (5) is a chemical decomposition process, known as Hoffman elimination and cannot be decoupled from water reduction, whereas Eq. (6) is an electrochemical reaction that depends on the applied potential.

$$C_5H_{14}NO^+ + OH^- \rightarrow C_3H_9N + C_2H_4O + H_2O \quad (5)$$

$$C_5H_{14}NO^+ + e^- \rightarrow C_5H_{14}NO\bullet \rightarrow C_3H_9N + C_2H_5O\bullet \quad (6)$$

At first sight, it is impossible to deduce and distinguish from the data presented in Fig. 1(a) to which extent the decomposition reaction proceeds throughout Eq. (5) or Eq. (6). In principle, the presence of additional water could shift the reaction presented in Eq. (6) to more positive potentials due to the changes at the interface and increased ion mobility (see Supporting Information, Table 1).

To understand the effect of the water content and applied potential in the formation and growth of Ni films from 1ChCl:2U DESs on low carbon steel, a set of potentiostatic electrodeposition experiments was performed at different overpotentials and water concentrations. The inset of Fig. 1(b) shows the CAs registered during Ni electrodeposition with 2.1 *wt%* of water within the potential range of $E = -0.70V$ to $-1.10V$.

In all cases, j-t transients have the same characteristic regions as these reported in many potentiostatic electrodeposition experiments, also from DESs [23,25,37,49]. The first interval consists of a monotonically decaying current which is followed by a stable, almost zero current period of time, which ranges from 1.5 s for $E = -1.10V$ to 170 s for $E = -0.70V$. During this time, denoted

induction time t_{ind}, the current is not solely due to double layer charging, but discharge of ions into adatoms, probably accompanied by formation of small nanoclusters [50–52]. After the induction interval, the absolute current value begins to increase due to growth by direct attachment and reaches a maximum, indicating 3D diffusion-limited or mixed kinetic-diffusion controlled growth. When the overpotential is very low (for $E = -0.70V$), the current starts to increase noticeably only after 200 s, indicating the very long t_{ind} and very slow kinetics [53]. This phenomenon points out that, in this type of solvents, performing cyclic voltammetry measurements at relatively slow scanning rates (10 mV/s) is still too fast to capture the slow kinetic processes (Fig. 1(a)). After reaching the current peak, the current decreases again and follows $I\alpha t^{0.5}$ (Cottrell) relation, which is typical for diffusion limited processes. However, for $E < -0.95V$, the current deviates from Cottrellian behaviour after a certain time, which is shorter for higher overpotentials (yellow curve of the inset in Fig. 1(b)) and reaches a plateau. This phenomenon indicates the contribution of additional electrochemical processes into the overall current, similar to what has been reported previously for the electrodeposition of cobalt with concomitant proton reduction [54] or, more recently, for the electrodeposition of chromium from a choline chloride-ethylene glycol DES with concomitant reduction of water [55]. In the present manuscript, the current arises from the reduction of water on the Ni growing centers.

The main graph of Fig. 1(b) shows the CAs registered during electrodeposition at $E = -0.90V$ from electrolytes containing different water contents. For the j-t curves recorded outside the glovebox, the current peak shifts to shorter times and higher currents, and the induction time decreases for increasing amounts of water (blue - 2.1 *wt%*, black - 4.5 *wt%* and red - 7.5 *wt%* curves), respectively. Alternatively, the trend is inverted for the CA recorded under glovebox conditions (0.1 *wt%*). The induction time is, in this case, lower than for 2.1 *wt%* of water. This is in line with the evolution of the onsets of Ni^{2+} reduction with water content (Fig. 1(a)). For low water contents, the decrease of the induction time with a decrease of water concentration from 2.1 *wt%* to 0.1 *wt%* would be explained by the appearance of a mixture of a tetrahedral and octahedral coordinated nickel in the latter conditions (see Supporting Information, Fig. S1). For higher H_2O concentrations, the decrease of t_{ind} with increasing water content could be explained by an increase of ion mobility (see Supporting Information, Table 1). In both cases, changes of the interfacial structure (i.e. higher concentration of water molecules) could also have an effect, although not yet possible to predict in which direction [45].

3.2. Influence of applied potential on the morphology and chemical composition of Ni coatings

Ni coatings were first deposited on low carbon steel substrates from 1ChCl:2U containing 0.2 M $NiCl_2 \cdot 6H_2O$ and 2.1 %*wt* of water. The films were formed by applying a constant potential ($E = -0.70V$ to $-1.10V$) for 45 min at 60 °C. A macroscopic difference between the appearance of deposited nickel coatings was evident and is recorded in the form of bright field optical microscopy images (Fig. 2). The visible change of the color already indicates differences in the chemical composition of the Ni films. The light grey shade visible in Fig. 2(a) is typical for metallic Ni structure, black color (Fig. 2(b)) is related with non-stochiometric nickel oxide/oxyhydroxide and light green (Fig. 2(c)) with nickel hydroxide [56,57].

Moreover, FE-SEM images of the surface and cross-sections were recorded in combination with EDS measurements. Characteristic images are presented in Figs. 3 and 4.

The FE-SEM images revealed that the electroplated Ni coatings have a compact and dense structure, which covers well the rough steel substrate (Fig. 3(a) and (b) in comparison with Fig. 3(d)). Moreover, it was observed that by varying the applied potential, the

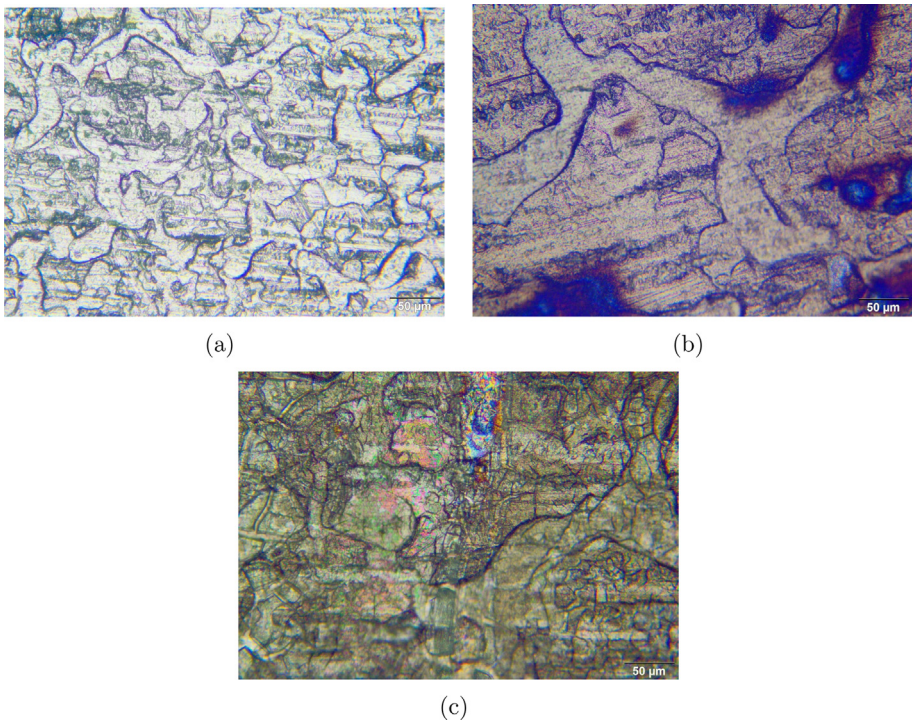

Fig. 2. Representative bright field optical microscopy images of Ni coatings deposited from 1ChCl:2U containing 0.2 M $NiCl_2 \cdot 6H_2O$ and 2.1 %*wt* of water at: (a) $E = -0.70V$, (b) $E = -0.90V$, (c) $E = -1.10V$.

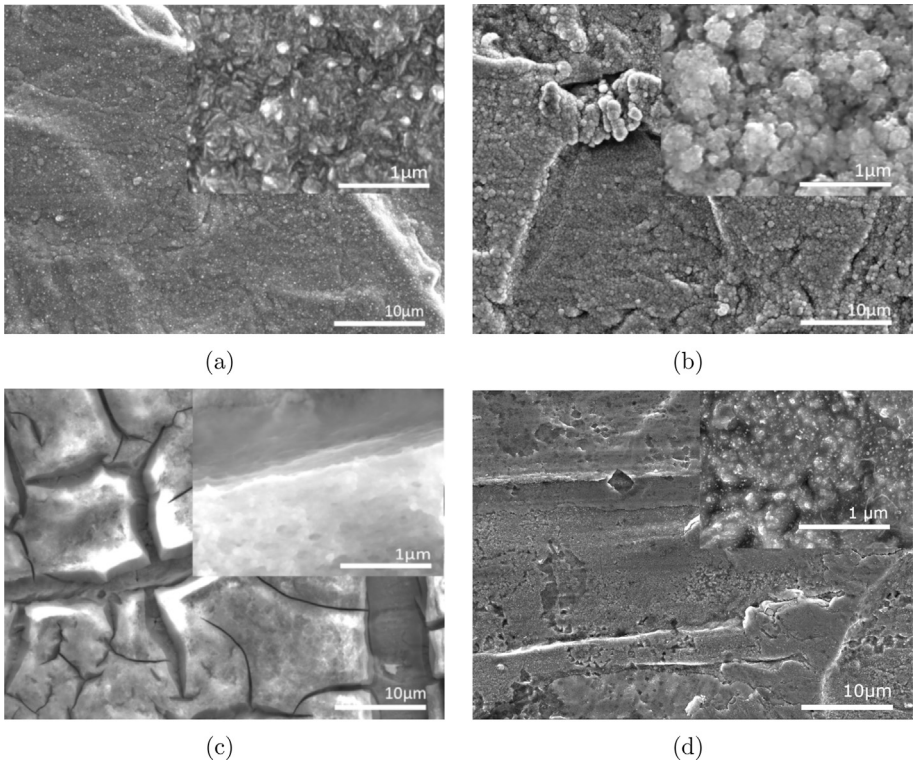

Fig. 3. Top-view FE-SEM images of Ni coatings deposited from 1ChCl:2U containing 0.2 M $NiCl_2 \cdot 6H_2O$ and 2.1 *wt%* of water at: (a) $E = -0.70V$, (b) $E = -0.90V$, (c) $E = -1.10V$ and (d) low carbon steel substrate.

morphology changes from pellet-like (Fig. 3(a)) to cauliflower-like (Fig. 3(b) and (c)) for films deposited at $E = -0.70V$, $E = -0.90V$ and $E = -1.10V$, respectively. Interestingly, in the case of the deposits formed at the highest overpotentials, the cauliflower-like nickel particles are completely covered by a cracked and porous (sponge-like) film.

The cross-section images (Fig. 4(a), (c) and 4(e)) revealed a cracked, discontinuous and non-uniform film throughout its thickness, whose thickness ranges from ~700 nm to 2.90 μm for deposits at $E = -0.70V$ and $E = -1.10V$, respectively. The sponge-like film observed in Fig. 3(c) gives a strong charging effect visible in the cross-section image (Fig. 4(e)), which indicates the presence of a non-conductive layer. This can be explained by a possible incorporation of electrolyte decomposition products. These by-products could be produced by the chemical decomposition of choline cation (Eq. (5)) once there is an excess of OH^- formed by surface limited reduction of water (as in Eq. (2), for $E \leq -0.99V$) and/or by and electrochemical route (Eq. (6), for $E \leq -1.10V$) (see Fig. 1(a)). Furthermore, defects in Ni films, such as cracks and detachments (Fig. 4(c) and (e)) are most likely caused by internal stresses, which may originate from disruptions in the lattice due to incorporation of Cl^- and absorption of hydrogen within the coating [1].

Further, EDS analysis was performed on the surface and cross-sections of the electrodeposited nickel coatings. The obtained results revealed the presence of Ni, C, O and Fe in the samples formed at $E = -0.70V$ and $E = -0.90V$. Additionally, a minimal concentration of Cl was detected in the coatings deposited at $E = -1.10V$, indicating that when choline decomposition occurs and possibly incorporates in the Ni coating, Cl gets trapped in the Ni film as well. The EDS line scan analysis performed on the cross-sections, presented in Fig. 4(b), (d) and 4(f), shows an interesting trend. When the thickness of the Ni film reaches about 350–450 nm (counting from the surface of the coating, at the right hand side of the EDS linescans), the Ni content starts to decrease whereas the concentration of O and C increases. This again indicates a possible incorporation of DESs components (or DES decomposition products) into the coating. It must be noted that very high concentrations of O and C throughout the cross-sectioned coating may partially originate from the sample preparation and exposure to the air. Furthermore, iron was detected at two ends of the deposit due to the high roughness of the steel substrate.

In order to resolve the chemical state of Ni within the coatings formed at different overpotentials, XPS measurements were performed on samples deposited at $E = -0.70V$, $E = -0.90V$ and $E = -1.10V$, at the outer surface and throughout depth, after sputtering. Fig. 5(a) presents an example of the XPS survey obtained at the outer surface and after different sputtering depths of the Ni coating formed at $E = -0.90V$ from 1ChCl:2U DESs containing 0.2 M $NiCl_2 \cdot 6H_2O$ and 2.1 *wt%* of water. The recorded XPS surveys confirmed the presence of Ni, O, C and Cl, also detected by EDS. It is evident that the presence of oxygen is not only due to the oxidation of the Ni coating in contact with the air since O can be detected all throughout the thickness of the Ni film. Recorded high-resolution spectra for samples deposited at $E = -0.70V$ and $E = -1.10V$ are presented in the Supporting Information (Figs. S2 and S3). Spectra registered for the deposits obtained at the highest overpotential do not reveal significant differences to the ones obtained at $E = -0.90V$. This is not the case for the coating electrodeposited at the lowest overpotentials ($E = -0.70V$), where the spectra obtained after sputtering 7.84 nm showed no presence of oxidized and/or hydroxylated Ni species but only metallic Ni. This indicates that oxidized Ni species detected on the outer surface (before sputtering) are formed during air exposure.

The analysis of survey depth profile (Fig. 5(b)) shows an increase of Ni and a decrease of O, C, Cl and N, with sputtering depth in the outermost layers (roughly 80 nm), before reaching a plateau. Once

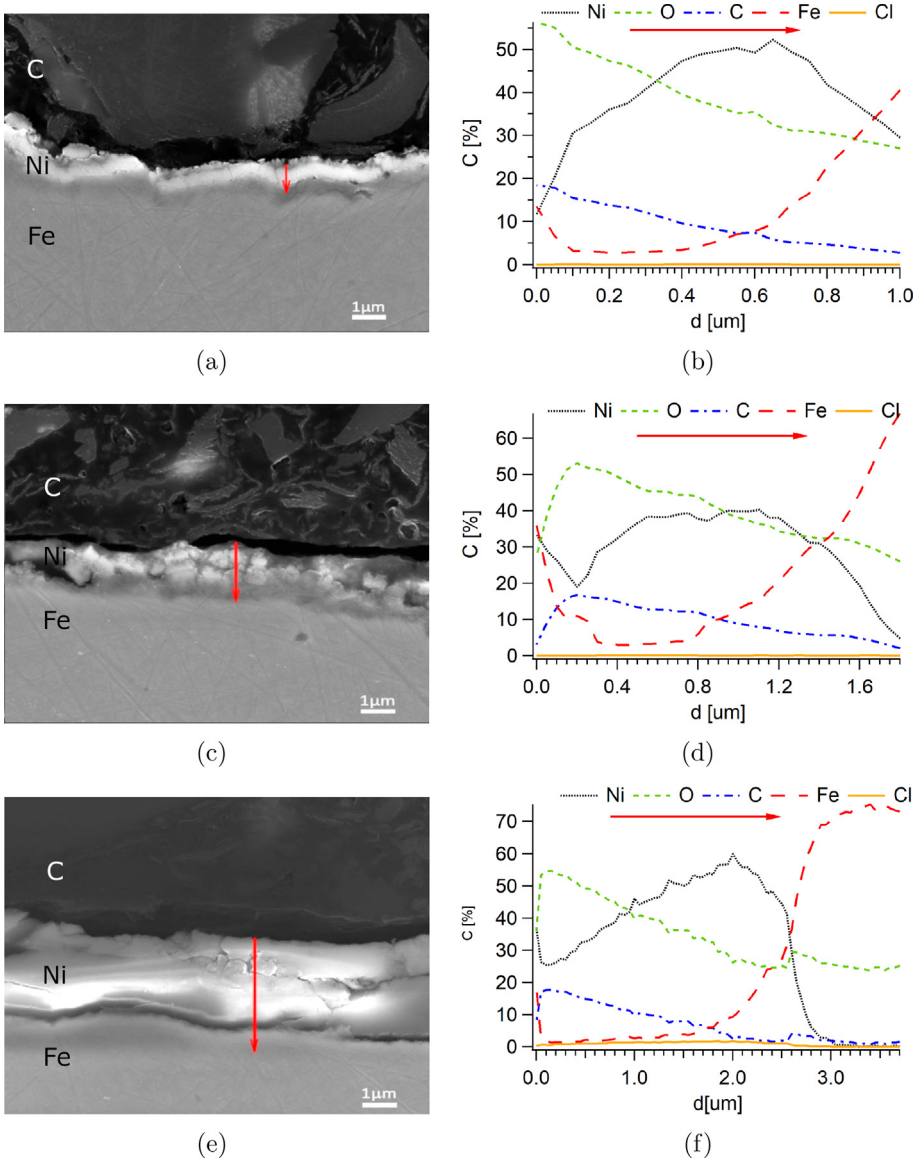

Fig. 4. EDS line scan analysis (marked with red arrow) of the cross-section of Ni coatings deposited from 1ChCl:2U DES containing 0.2 M $NiCl_2 \cdot 6H_2O$ and 2.1 *wt%* of water at: (a) and (b) $E = -0.70V$, (c) and (d) $E = -0.90V$ and (e) and (f) $E = -1.10V$; Ni – nickel coating, Fe – steel substrate, C – polymer resin. (For interpretation of the references to color in this figure legend, the reader is referred to the Web version of this article.)

~270 nm of material is sputtered, the concentration of Ni decreases and is no longer detected (~470 nm), indicating a transition region where Ni was deposited on the rough surface of steel. The analysis of the XPS surveys in function of sputtered depth showed similar trends for C and O concentration profiles as the EDS line scans. This leads to the conclusion that the oxygen signal does not come only from oxidized nickel, since it clearly increases (and decreases) as the carbon signal does. Therefore, this reinforces the idea that DES components (or DES decomposition by-products), containing both C and O are incorporated in the Ni film. To gain information on the chemical state of the detected elements, a series of high-resolution spectra were recorded and analysed.

Fig. 6 shows the spectra for the binding energy range E_{be} = 850 eV to 870 eV, which corresponds to the Ni2p3/2 orbital. The fitting of the nickel spectra indicates that the Ni2p3/2 orbital consists of three components, whose main peaks appear at E_{be} = 852.7 eV, E_{be} = 853.7 eV and E_{be} = 854.6 eV and are ascribed to metallic Ni, NiO and NiOOH, respectively. The last two Ni compounds indicate the presence of non-stochiometric nickel oxide-hydroxide, $NiO_x(OH)_{2(1-x)}$, as pure NiOOH can be formed only by applying high positive potentials [26,58]. After sputtering 7.84 nm (Fig. 6(b)) a large decrease in the concentration of nickel oxide-hydroxide species and an increase of pure Ni was revealed. This indicates that a large part of the oxidized Ni compounds detected on the outer surface of the coating were formed during the sample exposure to the atmosphere. Further analysis of the Ni2p3/2 spectra showed that, until certain sputtered depth, ~274.4 nm (Fig. 6(d) and (e)), the coating is composed of a mixture between metallic nickel and its oxide-hydroxide species, whereas at greater depths, the films consist almost purely of metallic Ni and some traces of Ni hydroxylated compound. This indicates that oxidized and hydroxylated Ni compounds were formed during the electrodeposition process [26,59,60]. The analysis of the O1s spectrum (see Supporting Information, Fig. S4) proved the presence of both oxides and hydroxides, as well as H_2O within almost the whole thickness of the coating.

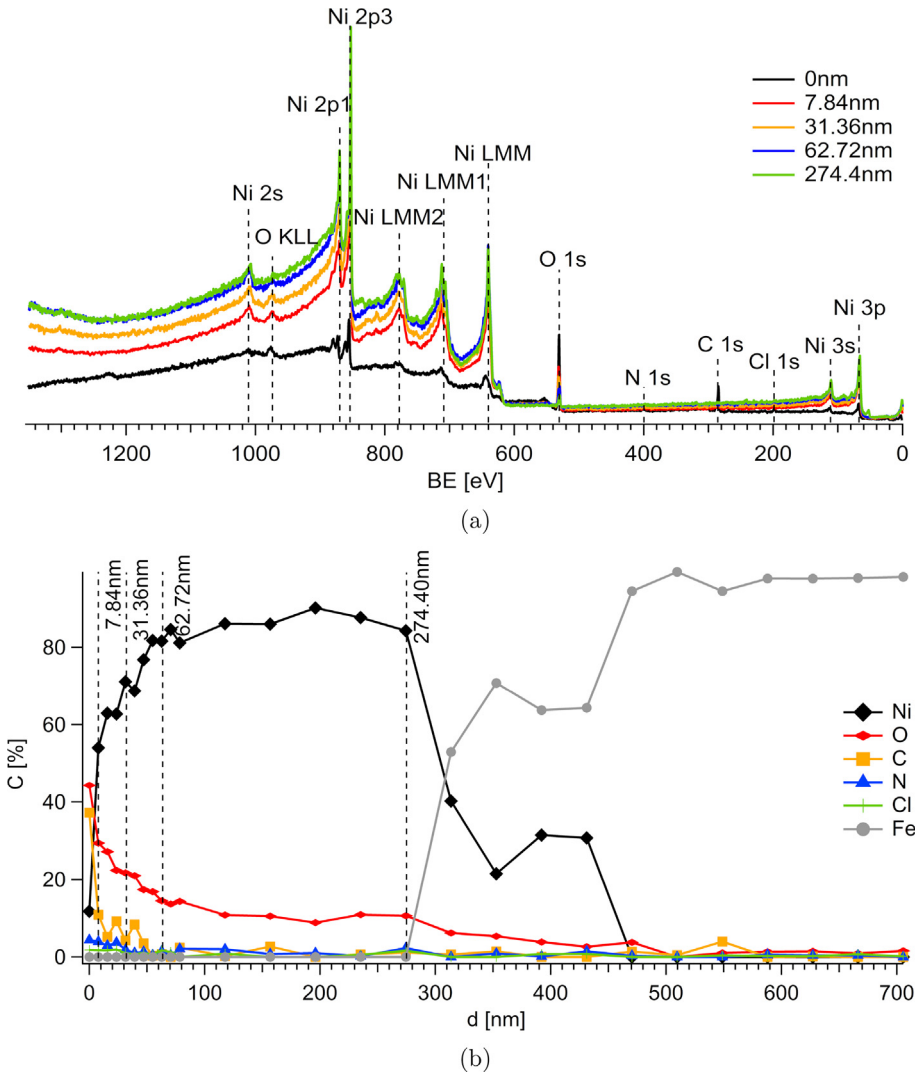

Fig. 5. XPS analysis of Ni film deposited at $E = -0.90V$ from 1ChCl:2U DESs containing 0.2 M $NiCl_2 \cdot 6H_2O$ and 2.1 *wt%* of water: (a) depth profile survey: 0 nm, 7.84 nm, 31.36 nm, 62.72 nm and 274.4 0 nm; b) elemental concentration depth profile.

In addition, Raman spectroscopy measurements were performed in specimens deposited at potentials of $E = -0.70V$ to $-1.10V$ from $NiCl_2 \cdot 6H_2O$ and 2.1 *wt%* of water containing DESs (Fig. 7).

The red and yellow curves, which represent the films formed at $E = -0.70V$ and $E = -0.80V$, respectively, show a very broad peak at ~530 cm^{-1}, marked as region A. Furthermore, a broad shoulder, marked as region D at a Raman shift of ~560 cm^{-1}, appears together with a weak and broad peak at ~3580 cm^{-1}, denoted region C. By applying a deposition potential of $E = -0.90V$ (green curve in Fig. 7), this shoulder (region D) disappears and the peak visible in region A narrows down. As the applied potential moves to $E = -0.95V$ and $E = -1.10V$ (blue and black curves, respectively), the peak in region A remains but the appearance of an additional set of vibrations between region D and C is detected. Interestingly, in the case of the sample formed at $E = -1.10V$ (black curve in Fig. 7), two broad and intense peaks at Raman shifts higher than 3100 cm^{-1} appear (marked as region B). The shallow and broad peaks in region C indicate the presence of free hydroxyl group and crystallized water [61]. Further analysis of the peaks detected between 600 cm^{-1} and 3100 cm^{-1} (between region D and C in Fig. 7) evidences the presence of organic compounds. The peaks present within 2750 cm^{-1} and 3100 cm^{-1} (region B) correspond to -CH_3 and -CH_2- vibrations, which are present in 1ChCl:2U mixture [62]. However, the vibrations visible between 650 cm^{-1} and 1500 cm^{-1} correspond to methyl and ethyl groups, whose positions and intensities are not the same as the ones in 1ChChl:2U solution. A further analysis of these peaks and the peak related to -OH group, indicates the presence of trimethylamine which is a choline decomposition product formed via the Hoffman elimination reaction [48]. The Raman shift peak visible in region A is related to the presence of NiO [63,64]. However, its broadness and the lack of second order overtones may indicate that the nickel oxide is amorphous or disordered [61]. Moreover, the occurrence of a weak shoulder, marked as region D, together with a shallow and broad peak in region C may be assigned to the presence of hydroxylated Ni species, such as NiOOH or $Ni(OH)_2$, however more likely $NiO_x(OH)_{2(1-x)}$ [65].

Both XPS and Raman data complete each other and indicate that electrodeposited Ni films are composed not only from metallic Ni but also nickel oxide-hydroxide and incorporated choline and its decomposition products, such as trimethylamine and acetaldehyde.

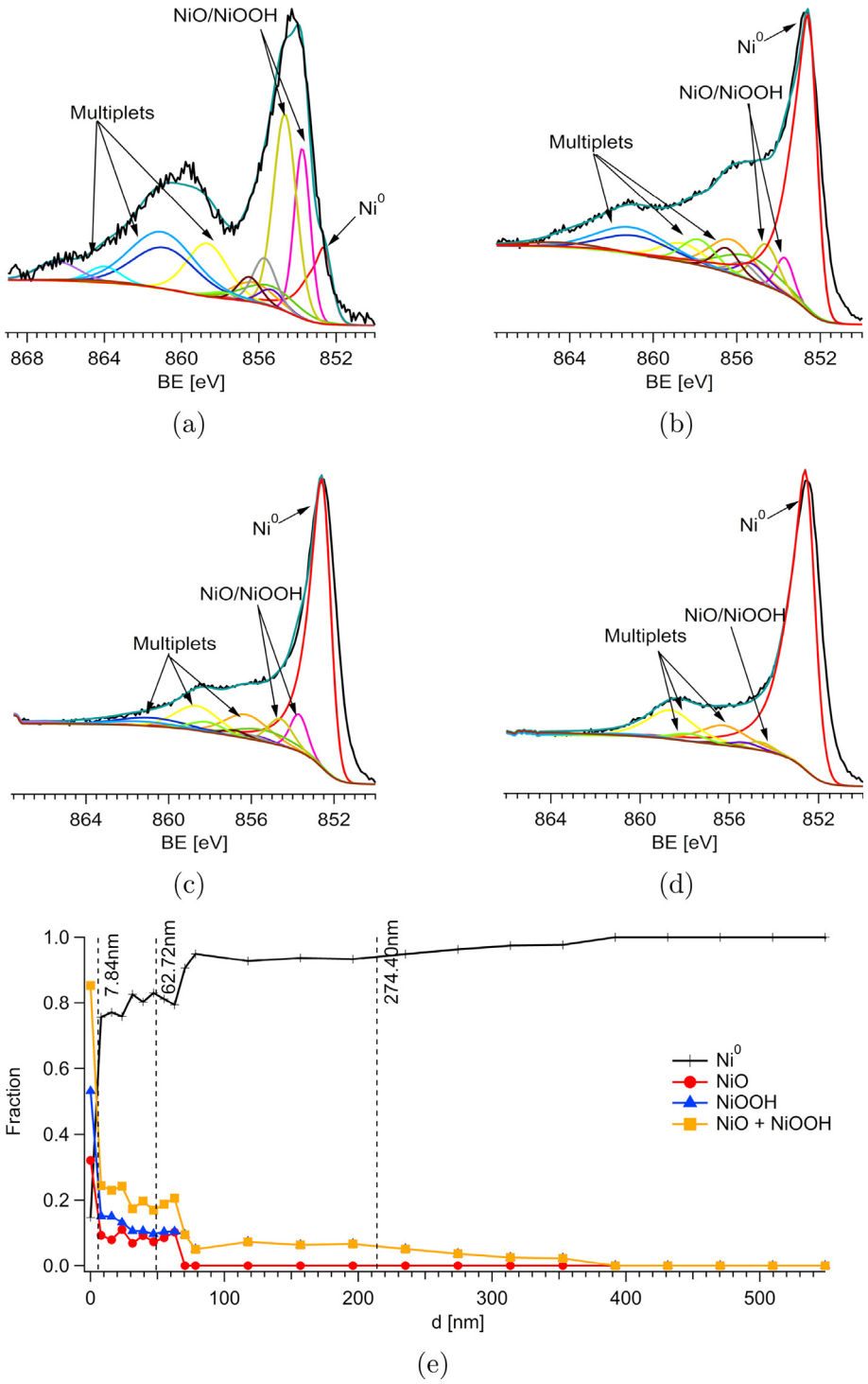

Fig. 6. XPS high-resolution spectra analysis of Ni2p3/2 in function of sputtered depth (a) 0 nm, (b) 7.84 nm, (c) 62.72 nm and (d) 274.4 nm of Ni film deposited at $E = -0.90V$ from 1ChCl:2U containing 0.2 M $NiCl_2 \cdot 6H_2O$ and 2.1 *wt%* of water. (e) Ni, Ni^{2+} and Ni^{3+} fraction in function of sputtered depth.

3.3. Influence of water content on the morphology and chemical composition of electrodeposited Ni films

Ni coatings were potentiostatically electrodeposited at $E = -0.90V$ for 45 min at 60 °C from 1ChCl:2U DESs containing 0.2 M of $NiCl_2 \cdot 6H_2O$ and different water content. Its concentration in the electrolyte was determined by Karl Fischer titration and the total values were: 2.1 *wt%*, 4.5 *wt%* and 7.5 *wt%*. The obtained films featured macroscopic differences in their appearance, similarly to the samples discussed in Section 3.2. Bright field images obtained by optical microscope presented in Figs. 2(b) and 8 show that the increase of water content in the electrolyte, from 2.1 *wt%* to 4.5 *wt%* and 7.5 *wt%*, changes the color and macroscopic morphology of the films from dull grey, through black, to light greenish and cracked films, respectively. The addition of water, up to 7.5 *wt%*, shifts H_2O reduction to more positive potentials, and thus an accumulation of

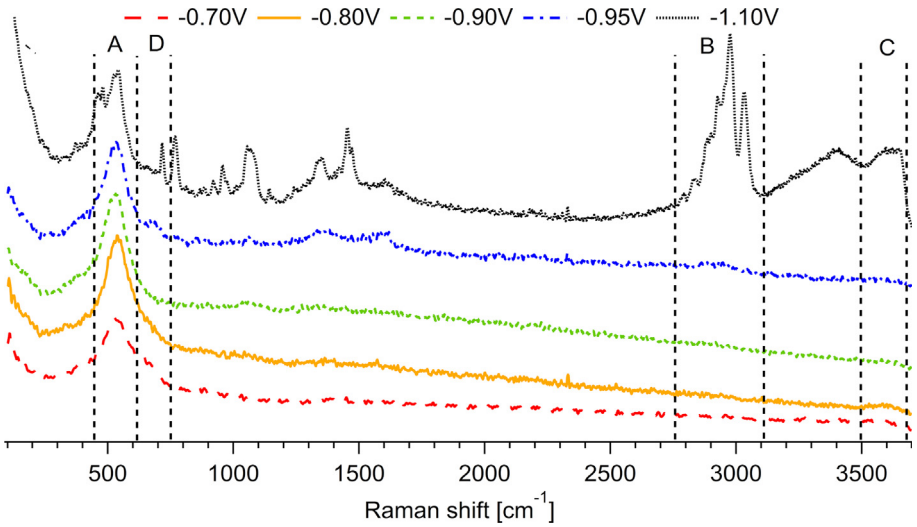

Fig. 7. Raman spectra of Ni films electrodeposited from 1ChCl:2U containing 0.2 M $NiCl_2 \cdot 6H_2O$ and 2.1 *wt%* of water at potentials ranging from $E = -0.70V$ to $-1.10V$.

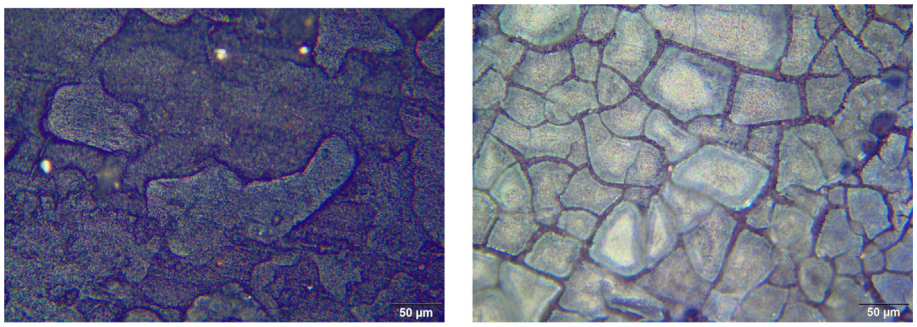

Fig. 8. Representative optical microscopy images of Ni coatings deposited at $E = -0.90V$ from DESs containing 0.2 M $NiCl_2 \cdot 6H_2O$ and: (a) 4.5%*wt* and (b) 7.5%*wt* of water.

OH^- occurs at the interface, which leads to the formation of oxidized and hydroxylated Ni species. Moreover, the excess of OH^- will force the chemical decomposition of choline cation, which proceeds via Eq. (5). These phenomena, water and choline reduction at lower overpotentials, result in the macroscopic changes in the Ni coating appearance [27].

The deposits were analysed by FE-SEM and EDS. The results are shown in Figs. 3(b), 4(c) and 4(d) and 9.

Fig. 9(a) and (b) revealed that, for 4.5 *wt%* and 7.5 *wt%* of water, the Ni surface consists of particles larger than 700 nm that are embedded in a cracked film. These particles grow in cauliflower shape and do not form compact layers. The cross-section images, presented in Fig. 9(c) and (d), show that, for 4.5 *wt%* water content, a thin, non-uniform and discontinuous Ni film with a thickness of ~500 nm, was deposited. Above this layer, a few μm thick film with non-conductive properties (visible charging effect) was formed. Single and irregular-shaped particles were embedded in this film. Alternatively, for 7.5 *wt%* (Fig. 9(d)), a non-uniform Ni layer of a thickness of ~200–250 nm was deposited and above which a thick and continuous non-conductive film was formed. Such film clearly prevents further growth of the Ni coating. These observations are similar to those made for coatings electroplated at higher overpotentials ($E = -1.10V$) from an electrolyte with lower water content (2.1 *wt%*) (Fig. 4(e)).

Fig. 9(e) and (f) show EDS linescans performed in the place marked with the red arrow in Fig. 9(c) and (d). Ni, C, O, Fe and Cl are detected, as expected. The elemental concentration profiles are similar to these described in Section 3.2.

In addition, XPS measurements were performed for the deposited films with different water contents (4.5 *wt%* and 7.5 *wt%*). The spectra are very similar to these of Section 3.2. (Fig. 5(a)) and are included in the Supporting Information (Section 3, Figs. S6 and S7). Ni, O, C, Cl, N and Fe were detected in all the samples. Fig. 10(a) shows the elemental concentration profile in function of depth and reveals that the films obtained from 1ChCl:2U DESs containing 7.5 *%wt* water are much thicker and contain a higher concentration of O, C, Cl and N than the ones obtained from the electrolyte with only 2.1 *%wt* of water. Furthermore, O and C followed similar trends to these observed earlier in section 3.2. Their concentration decreases with the increase of sputtered thickness, whereas Ni content increases. At a sputtered depth of ~200 nm, a plateau was reached for the concentration of all detected elements, which indicates that their presence is not related to sample exposure to the air, especially not the presence of oxidized and hydroxylated Ni species (Fig. 10(b)).

The analysis of Ni2p3/2 high-resolution spectra revealed a similar composition to these presented in Fig. 6(a)–6(d). In all of the cases, metallic Ni mixed with nickel oxide-hydroxide was detected, which was confirmed by analysing O1s spectrum (see Supporting Information, Fig. S7).

Once more, the XPS data was compared with Raman spectroscopy. Fig. 11 shows that the Ni coating deposited from DESs

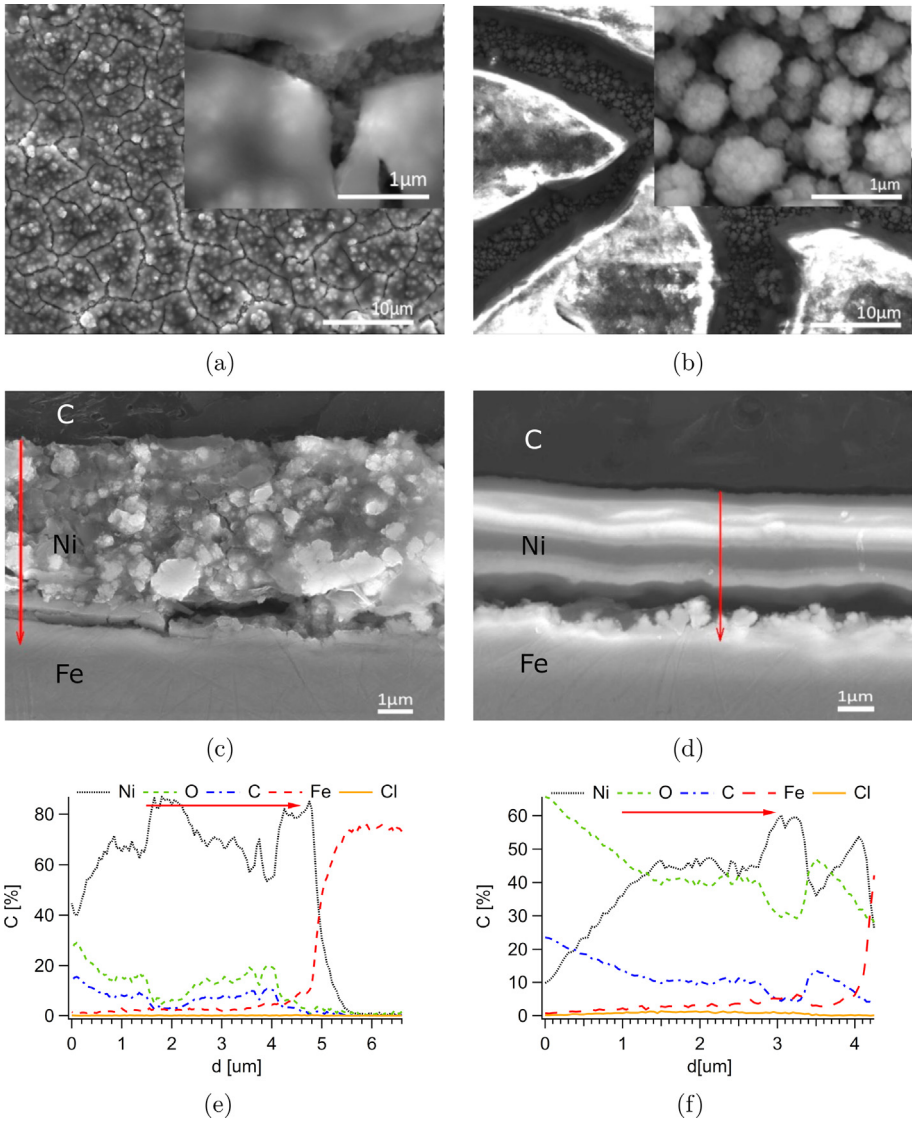

Fig. 9. Top-view and cross-section FE-SEM images with EDS line scans (marked with red arrow) for Ni coatings deposited at $E = -0.90V$ from DESs containing 0.2 M $NiCl_2 \cdot 6H_2O$ and: (a), (c), (e) 4.5 *wt%* and (b), (d), (f) 7.5 *wt%* of water; Ni – nickel coating, Fe – steel substrate, C – polymer resin. (For interpretation of the references to color in this figure legend, the reader is referred to the Web version of this article.)

containing only 2.1 *wt%* of water (black curve) shows only one broad peak appearing within the Raman shift range between 410 cm^{-1} and 610 cm^{-1}, marked as region A. By increasing the amount of water up to 4.5 *wt%* (blue curve), a weak and broad shoulder appears in region A. Furthermore, very shallow peaks show up at Raman shifts of 2750 cm^{-1} to 3090 cm^{-1}, marked as region B and between 3500 cm^{-1} to 3700 cm^{-1}, region C. Some barely visible traces are present in the Raman shift range between 610 cm^{-1} and 2750 cm^{-1}. All these bands are intensified when the deposition is performed in an electrolyte containing 7.5 *wt%* of water (red curve) and the intensity of the peak in region A (~500 cm^{-1}) decreases.

Figs. 7 and 11, show many similarities. The broad peak in the region A and the lack of second order overtones indicate that NiO is most likely present in an amorphous and disordered form. The shoulder in region A together with the shallow peak at high Raman shifts may indicate the evidence of an hydroxylated form of nickel. This is especially visible in the case of the red curve (7.5 *wt%* water), which is very similar to the Raman spectrum obtained for the sample deposited at $E = -1.10V$ from DESs containing only 2.1 *wt%* of water (Fig. 7).

In the Raman shift range between 610 cm^{-1} and 3090 cm^{-1}, bands related to -CH_3 and -CH_2- groups are detected. These bands can be assigned to the choline cation, and trimethylamine that is being formed during the decomposition process of choline via Hoffman elimination (Eqs. (5) and (6)). This proves that performing electrodeposition of Ni in the presence of more than 4.5 *%wt* of water in 1ChCl:2U DESs enhances the decomposition of the electrolyte and inhibits the growth of Ni coating.

3.4. Suggested deposition mechanism

The data presented in the previous sections indicates the complexity of Ni electrodeposition from 1ChCl:2U DESs on low carbon steel. The analysis of cyclic voltammograms and chronoamperograms showed the inter-relation between applied potential and water content in the electrolyte. As observed in the CVs (Fig. 1(a)) and presented in Fig. 12, Ni^{2+} reduction is accompanied

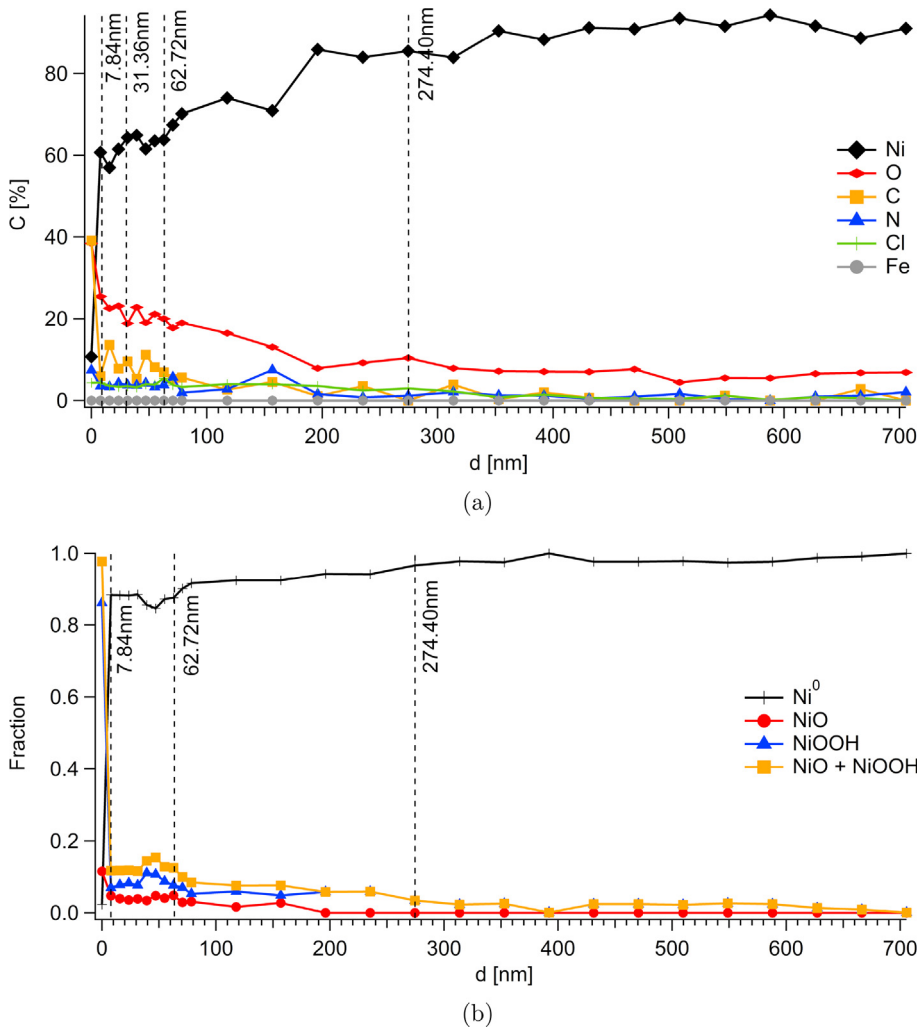

Fig. 10. (a) Concentration profile of a Ni film, sputtered up to 700 nm from the surface, deposited at $E = -0.90V$ from an electrolyte containing 0.2 M $NiCl_2 \cdot 6H_2O$ and 7.5 *%wt* water.(b) Ni, Ni^{2+} and Ni^{3+} fraction in function of sputtered depth of Ni coating deposited at $E = -0.90V$ from DESs containing 7.5 *wt%* water.

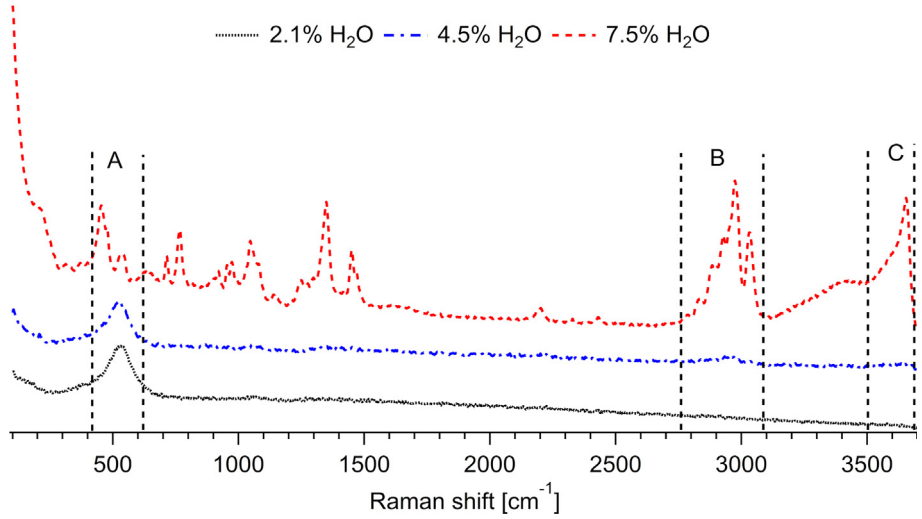

Fig. 11. Raman spectra of Ni coatings electrodeposited from 1ChCl:2U DES containing 2.1 *wt%*, 4.5 *wt%* and 7.5 *wt%* water at 60 °C and E = – 0.90*V*.

by water splitting. This is the cause of most of the morphological issues of the coatings, such as brittleness, cracks, pores, and lack of adhesion. An analysis of the onset potentials of Ni^{2+} and water reduction, for different water contents, is presented in Fig. 12 and

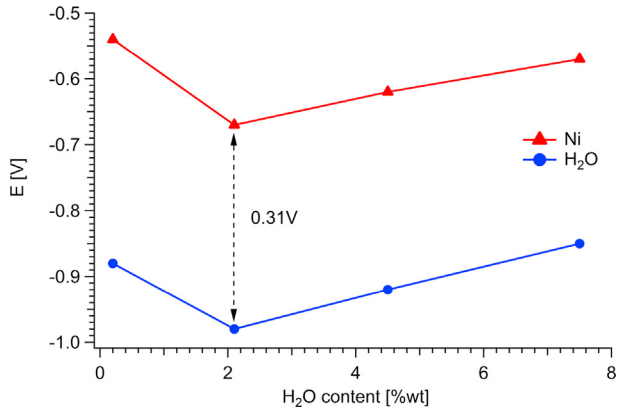

Fig. 12. The onset potential for Ni^{2+} and H_2O reduction in function of water content in 1ChCl:2U DESs.

reveals the difficulties of decoupling these two reactions.

The mechanism of electrochemical formation of Ni coatings from 1ChCl:2U DESs containing different amounts of water and/or at different applied potentials is presented schematically in Fig. 13. By performing electrodeposition at low overpotentials ($E = -0.70V$ to $-0.80V$) and in low-water-content electrolytes ($\leq$4.5 *wt*% H_2O), it is possible to reduce Ni^{+2} (Fig. 13.1) and grow uniform, compact, layer-structured and crack-free films (Fig. 13.2). EDS, XPS and Raman spectroscopy results revealed that, as the water content increases ($\geq$4.5 *wt*% H_2O) and the applied potential becomes more negative ($E \leq -0.90V$), a rapid increase of C and O, and a decrease of the Ni concentration occurs throughout the thickness of the deposit, which is a mixture between metallic and oxide-hydroxide nickel species. The formation of mixed oxidized and hydroxylated Ni compounds can be explained, as described in section 3.1, by the adsorption of OH^- (Eq. (3)), which is formed during water reduction (Eqs. (2) and (4) [25,26]) (Fig. 13.3–13.5). This reaction can be catalysed by the presence of Ni particles on the steel substrate and/or by applying higher overpotentials. Interestingly, the surface analysis measurements evidenced the incorporation of choline and its decomposition products in the coating. Once there is an excess of hydroxyl group at the surface, the decomposition of 1ChCl:2U DESs proceeds via the Hoffman elimination reaction (Eq. (5)) [48]. Furthermore, the breakdown of the electrolyte is also known to be triggered by applying high overpotentials, which provokes the reaction described in Eq. (6) (Fig. 13.5 and 13.6). Both DESs decomposition reactions lead to the incorporation of organic compounds, such as trimethylamine, acetaldehyde and trapping choline in the deposited films.

4. Conclusions

The inter-related effect of applied potential and water content on the electrodeposition of Ni coatings from 1ChCl:2U DES on low carbon steel was studied by electrochemical measurements and surface analysis. Both applied potential and water content are crucial since they highly influence the morphology and chemical composition of the deposited coatings. A water content higher than 4.5 *%wt* and/or performing electrodeposition at potentials more negative than $E = -0.90V$ enhances the decomposition of the solvent. This breakdown appears via either an electrochemical and/or chemical reaction triggered by water reduction. In both cases, it leads to the incorporation of DES decomposition products, such as aldehydes and amines within the deposited Ni film. Moreover, the coatings obtained under these conditions are composed of metallic Ni and $NiO_x(OH)_{2(1-x)}$. The presence of this mixture is strictly related to the presence of residual and additional water in DES, which gets reduced when applying a sufficiently negative potential.

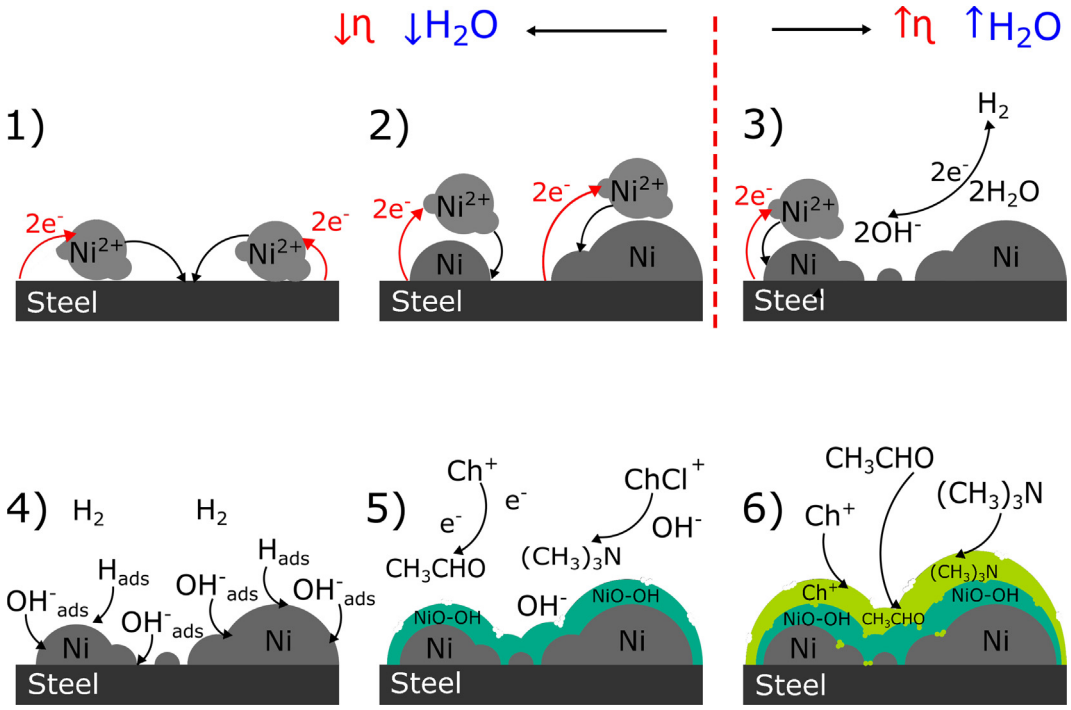

Fig. 13. Ni coating growth mechanism: 1. reduction of Ni cations; 2. formation of Ni nuclei and film growth; 3. further growth of coating and water reduction; 4. adsorption of hydrogen, hydroxyl groups and formation of Ni oxide-hydroxide layer; 5. decomposition of DESs to trimethylamine, aldehydes, etc.; 6. incorporation of electrolyte decomposition products. The red arrows indicate electron transfer occurring during Ni^{2+} reduction, whereas the black ones the place where certain species can be found. (For interpretation of the references to color in this figure legend, the reader is referred to the Web version of this article.)

It has been evidenced that small amounts of H_2O affect complexation of Ni^{2+}, which further influences the electrodeposition process. Despite the complexity of the process, performing electrodeposition at low overpotentials ($E > -0.90V$) and low water contents ($< 4.5\ \%wt$) leads to the formation of adherent pure metallic Ni coatings.

Acknowledgements

E.A. Mernissi Cherigui acknowledges funding from the Fonds Wetenschappelijk Onderzoek in Flanders (FWO, research project G019014N). J. Ustarroz acknowledges funding from the Fonds Wetenschappelijk Onderzoek in Flanders (FWO, postdoctoral grant 12I7816N).

Appendix A. Supplementary data

Supplementary data to this article can be found online at https://doi.org/10.1016/j.electacta.2019.06.161.

References

[1] M. Schlesinger, M. Paunovic (Eds.), Modern Electroplating, 5th Edition, John Wiley and Sons, Inc., New Jersey, 2010.
[2] P. Sahoo, S.K. Das, Tribology of electroless nickel coatings – a review, Mater. Des. 32 (2011) 1760–1775.
[3] J. Vite-Torres, M. Vite-Torres, R. Aguilar-Osorio, J.E. Reyes-Astivia, Tribological and corrosion properties of nickel coatings on carbon steel, FME Transactions 43 (2015) 206–210.
[4] N. Sridhar, K. Udaya Bhat, Effect of deposition time on the morphological features and corrosion resistance of electroless Ni-high P coatings on aluminium, J. Mater. (2013) 1–7.
[5] A. Sahari, A. Azizi, G. Schmerber, A. Dinia, Nucleation, growth and morphological properties of electrodeposited nickel films from different baths, Surf. Rev. Lett. 15 (2008) 717–725.
[6] D.E. Rusu, A. Ispas, A. Bund, C. Gheorghies, G. Cârâc, Corrosion tests of nickel coatings prepared from a Watts-type bath, J. Coat. Technol. Res. 9 (2012) 87–95.
[7] T. Mimani, S.M. Mayanna, N. Munichandraiah, Influence of additives on the electrodeposition of nickel from a Watts bath: A cyclic voltammetric study, J. Appl. Electrochem. 23 (1993) 339–345.
[8] A. Rashidi, A. Amadeh, The effect of saccharin addition and bath temperature on the grain size of nanocrystalline nickel coatings, Surf. Coating. Technol. 204 (2009) 353–358.
[9] A. Ciszewski, S. Posluszny, G. Milczarek, M. Baraniak, Effects of saccharin and quaternary ammonium chlorides on the electrodeposition of nickel from a Watts-type electrolyte, Surf. Coating. Technol. 183 (2004) 127–133.
[10] A.P. Abbott, G. Frisch, K.S. Ryder, Electroplating using ionic liquids, Annu. Rev. Mater. Res. 43 (2013) 335–358.
[11] A. Ispas, A. Bund, Electrodeposition in ionic liquids, Electrochem. Soc. Interf. 23 (1) (2014) 47–51.
[12] S. LopezLeon, R. Ortega-Borges, G. Brisard, Nickel electrodeposition from protic ionic liquids based on carboxylate anions as electrolyte: II. electrodeposition from 2-hydroxyethyl ammonium propionate, Int. J. Electrochem. Sci. 8 (2013) 1382–1393.
[13] M. Deng, I. Sun, P. Chen, J. Chang, W. Tsai, Electrodeposition behavior of nickel in the water- and air-stable 1-ethyl-3-methylimidazolium-dicyanamide room-temperature ionic liquid, Electrochim. Acta 53 (2008) 5812–5818.
[14] Y. Zhu, Y. Katayama, T. Miura, Effects of coumarin and saccharin on electrodeposition of Ni from a hydrophobic ionic liquid, Electrochim. Acta 123 (2014) 303–308.
[15] A.P. Abbott, I. Dalrymple, F. Endres, D.R. Macfarlane, Electrodeposition from Ionic Liquids, Wiley-VCH Verlag GmbH & Co. KGaA, 2008.
[16] K. Haerens, E. Matthijs, A. Chmielarz, B. Van der Bruggen, The use of ionic liquids based on choline chloride for metal deposition: A green alternative? J. Environ. Manag. 90 (2009) 3245–3252.
[17] D.V. Wagle, H. Zhao, G.A. Baker, Deep eutectic solvents: Sustainable media for nanoscale and functional materials, Accounts Chem. Res. 47 (2014) 2299–2308.
[18] E.L. Smith, A.P. Abbott, K.S. Ryder, Deep eutectic solvents (DESs) and their applications, Chem. Rev. 114 (2014) 11060–11082.
[19] Q. Zhang, K. De Oliveira Vigier, S. Royer, F. Jérôme, Deep eutectic solvents: Syntheses, properties and applications, Chem. Soc. Rev. 41 (2012) 7108–7146.
[20] A.P. Abbott, K. El Ttaib, K.S. Ryder, E.L. Smith, Electrodeposition of nickel using eutectic based ionic liquids, Transactions of the IMF 86 (2008) 234–240.
[21] A.P. Abbott, A. Ballantyne, R.C. Harris, J. a. Juma, K.S. Ryder, G. Forrest, A comparative study of nickel electrodeposition using deep eutectic solvents and aqueous solutions, Electrochim. Acta 176 (2015) 718–726.
[22] D. Yue, Y. Jia, Y. Yao, J. Sun, Y. Jing, Structure and electrochemical behavior of ionic liquid analogue based on choline chloride and urea, Electrochim. Acta 65 (2012) 30–36.
[23] A.P. Abbott, A. Ballantyne, R.C. Harris, J.A. Juma, K.S. Ryder, Bright metal coatings from sustainable electrolytes: The effect of molecular additives on electrodeposition of nickel from a deep eutectic solvent, Phys. Chem. Chem. Phys. 19 (2017) 3219–3231.
[24] H. Yang, X. Guo, N. Birbilis, G. Wu, W. Ding, Tailoring nickel coatings via electrodeposition from a eutectic-based ionic liquid doped with nicotinic acid, Appl. Surf. Sci. 257 (2011) 9094–9102.
[25] P. Sebastian, M.I. Giannotti, E. Gomez, J.M. Feliu, Surface sensitive nickel electrodeposition in deep eutectic solvent, ACS Appl. Energy Mater. 1 (2018) 1016–1028.
[26] E.A. Mernissi Cherigui, K. Sentosun, P. Bouckenooge, H. Vanrompay, S. Bals, H. Terryn, J. Ustarroz, Comprehensive study of the electrodeposition of nickel nanostructures from deep eutectic solvents: Self-limiting growth by electrolysis of residual water, J. Phys. Chem. C 121 (2017) 9337–9347.
[27] E.A. Mernissi Cherigui, K. Sentosun, M. Haile Mamme, M. Lukaczynska, H. Terryn, S. Bals, J. Ustarroz, On the control and effect of water content during the electrodeposition of Ni nanostructures from deep eutectic solvents, J. Phys. Chem. C 122 (2018) 23129–23142.
[28] R. Bernasconi, L. Magagnin, Electrodeposition of nickel from DES on aluminium for corrosion protection, Surf. Eng. 33 (2017) 131–135.
[29] C. Gu, Y. You, Y. Yu, S. Qu, J. Tu, Microstructure, nanoindentation, and electrochemical properties of the nanocrystalline nickel film electrodeposited from choline chloride–ethylene glycol, Surf. Coating. Technol. 205 (2011) 4928–4933.
[30] A. Florea, L. Anicai, S. Costovici, F. Golgovici, T. Visan, Ni and Ni alloy coatings electrodeposited from choline chloride-based ionic liquids - electrochemical synthesis and characterization, Surf. Interface Anal. 42 (2010) 1271–1275.
[31] G. Cai, C. Gu, J. Zhang, P. Liu, X. Wang, Y. You, J. Tu, Ultra fast electrochromic switching of nanostructured NiO films electrodeposited from choline chloride-based ionic liquid, Electrochim. Acta 87 (2013) 341–347.
[32] A. Yadav, S. Pandey, Densities and viscosities of (choline chloride + urea) deep eutectic solvent and its aqueous mixtures in the temperature range 293.15 K to 363.15 K, J. Chem. Eng. Data 59 (2014) 2221–2229.
[33] V. Protsenko, A. Kityk, D. Shaiderov, F. Danilov, Effect of water content on physicochemical properties and electrochemical behavior of ionic liquids containing choline chloride, ethylene glycol and hydrated nickel chloride, J. Mol. Liq. 212 (2015) 716–722.
[34] C. Du, B. Zhao, X. Chen, N. Birbilis, H. Yang, Effect of water presence on choline chloride-2urea ionic liquid and coating platings from the hydrated ionic liquid, Sci. Rep. 6 (2016) 29225.
[35] D. Shah, F.S. Mjalli, Effect of water on the thermo-physical properties of Reline: An experimental and molecular simulation based approach, Phys. Chem. Chem. Phys. 16 (2014) 23900–23907.
[36] F.I. Danilov, V.S. Protsenko, A.A. Kityk, D.A. Shaiderov, E.A. Vasil'eva, U. Pramod Kumar, C. Joseph Kennady, Electrodeposition of nanocrystalline nickel coatings from a deep eutectic solvent with water addition, Protect. Met. Phys. Chem. Surface 53 (2017) 1131–1138.
[37] C. Du, H. Yang, X. Chen, L. Wang, H. Dong, Y. Ning, Y. Lai, J. Jia, B. Zhao, Effect of coordinated water of hexahydrate on nickel platings from choline–urea ionic liquid, J. Mater. Sci. 53 (2018) 10758–10771.
[38] K. Gong, Y. Hua, C. Xu, Q. Zhang, Y. Li, J. Ru, Y. Jie, Electrodeposition behavior of bright nickel in air and water-stable betaine HCl–ethylene glycol ionic liquid, Trans. Nonferrous Metals Soc. China 25 (2015) 2458–2465.
[39] S. Trasatti, Electrocatalysis: Understanding the success of DSA, Electrochim. Acta 45 (2000) 2377–2385.
[40] S.L. Perkins, P. Painter, C.M. Colina, Experimental and computational studies of choline chloride-based deep eutectic solvents, J. Chem. Eng. Data 59 (2014) 3652–3662.
[41] T. Zhekenov, N. Toksanbayev, Z. Kazakbayeva, D. Shah, F.S. Mjalli, Formation of type III Deep Eutectic Solvents and effect of water on their intermolecular interactions, Fluid Phase Equilib. 441 (2017) 43–48.
[42] P. Kumari, Shobhna, K. Supreet, K.K. Hemant, Influence of hydration on the structure of reline deep eutectic solvent: A molecular dynamics study, ACS Omega 3 (2018) 15246–15255.
[43] C. D'Agostino, M.D. Gladden, L.F. Mantle, A.P. Abbott, E.I. Ahmed, A.Y.M. AMurshedi, R.C. Harris, Molecular and ionic diffusion in aqueous – deep eutectic solvent mixtures: Probing inter-molecular interactions using PFG NMR, Phys. Chem. Chem. Phys. 17 (2015) 15297–15304.
[44] O.S. Hammond, D.T. Bowron, K.J. Edler, The effect of water upon deep eutectic solvent nanostructure: An unusual transition from ionic mixture to aqueous solution, Angew. Chem. Int. Ed. 56 (2017) 9782–9785.
[45] O.S. Hammond, H. Li, C. Westermann, F. Endres, A.Y.M. Al-Murshedi, A.P. Abbott, G. Warr, K.J. Edler, R. Atkin, Nanostructure of the deep eutectic solvent/platinum electrode interface as a function of potential and water content, Nanoscale Horizons 4 (2018) 158–168.
[46] C.D. Gu, J.P. Tu, Thermochromic behavior of chloro-nickel(II) in deep eutectic solvents and their application in thermochromic composite films, RSC Adv. 1 (2011) 1220–1227.
[47] M. Gong, W. Zhou, M. Tsai, J. Zhou, M. Guan, M. Lin, B. Zhang, Y. Hu, D. Wang, J. Yang, S. Pennycook, H. Hwang, B. Dai, Nanoscale nickel oxide/nickel heterostructures for active hydrogen evolution electrocatalysis, Nat. Commun. 5 (2014) 4695–4701.

[48] K. Haerens, E. Matthijs, K. Binnemans, B. Van der Bruggen, Electrochemical decomposition of choline chloride based ionic liquid analogues, Green Chem. 11 (2009) 1357–1365.
[49] J. Aldana-González, M. Romero-Romo, J. Robles-Peralta, P. Morales-Gil, E. Palacios-González, M. Ramírez-Silva, J. Mostany, M. Palomar-Pardavé, On the electrochemical formation of nickel nanoparticles onto glassy carbon from a deep eutectic solvent, Electrochim. Acta 276 (2018) 417–423.
[50] J. Ustarroz, X. Ke, A. Hubin, S. Bals, H. Terryn, New insights into the early stages of nanoparticle electrodeposition, J. Phys. Chem. C 116 (2012) 2322–2329.
[51] J. Ustarroz, J.A. Hammons, T. Altantzis, A. Hubin, S. Bals, H. Terryn, A generalized electrochemical aggregative growth mechanism, J. Am. Chem. Soc. 135 (2013) 11550–11561.
[52] M. Haile Mamme, C. Kohn, J. Deconinck, J. Ustarroz, Numerical insights into the early stages of nanoscale electrodeposition: Nanocluster surface diffusion and aggregative growth, Nanoscale 10 (2018) 7194–7209.
[53] P. Altimari, F. Pagnanelli, Electrochemical nucleation and three-dimensional growth of metal nanoparticles under mixed kinetic-diffusion control: Model development and validation, Electrochim. Acta 206 (2016) 116–126.
[54] M. PalomarPardavé, B. Scharifker, E. Arce, M. Romero-Romo, Nucleation and diffusion controlled growth of electroactive centers, Electrochim. Acta 50 (2005) 4736–4745.
[55] I. MejíaCaballero, J. Aldana-Gonzàlez, T.L. Manh, M. RomeroRomo, E.M. ArceEstrada, I. CamposSilva, M.T. RamírezSilva, M. PalomarPardavé, Mechanism and kinetics of chromium electrochemical nucleation and growth from a choline chloride/ethylene glycol deep eutectic solvent, J. Electrochem. Soc. 165 (2018) D393–D401.
[56] R.M. Bendert, D.A. Corrigan, Effect of coprecipitated metal ions on the electrochromic properties of nickel hydroxide, J. Electrochem. Soc. 136 (1989) 1369–1374.
[57] M. Fantini, A. Gorenstein, Electrochromic nickel hydroxide films on transparent/conducting substrates, Sol. Energy Mater. 16 (1987) 487–500.
[58] B. Beden, D. Floner, J. Léger, C. Lamy, A voltammetric study of the formation on hydroxides and oxyhydroxides on nickel single crystal electrodes in contact with an alkaline solution, Surf. Sci. 162 (1985) 822–829.
[59] A.P. Grosvenor, M.C. Biesinger, R.S. Smart, N.S. McIntyre, New interpretations of XPS spectra of nickel metal and oxides, Surf. Sci. 600 (2006) 1771–1779.
[60] I.G. Casella, M.R. Guascito, M.G. Sannazzaro, Voltammetric and XPS investigations of nickel hydroxide electrochemically dispersed on gold surface electrodes, J. Electroanal. Chem. 462 (1999) 202–210.
[61] G. Socrates, Infrared and Raman Characteristic Group Frequencies, Wiley, 2001.
[62] C. Yuan, K. Chu, H. Li, L. Su, K. Yang, Y. Wang, X. Li, In situ Raman and synchrotron X-ray diffraction study on crystallization of Choline chloride/Urea deep eutectic solvent under high pressure, Chem. Phys. Lett. 661 (2016) 240–245.
[63] P. Delichere, Electrochromism in nickel oxide thin films by OMA and Raman spectroscopy, J. Electrochem. Soc. 135 (1988) 1856–1857.
[64] B.S. Yeo, A.T. Bell, In situ Raman study of nickel oxide and gold-supported nickel oxide catalysts for the electrochemical evolution of oxygen, J. Phys. Chem. C 116 (2012) 8394–8400.
[65] D.S. Hall, D.J. Lockwood, S. Poirier, C. Bock, B.R. MacDougall, Raman and infrared spectroscopy of α and β phases of thin nickel hydroxide films electrochemically formed on nickel, J. Phys. Chem. A 116 (2012) 6771–6784.